International Journal of Thermal Sciences 48 (2009) 1223–1234

Contents lists available at ScienceDirect

International Journal of Thermal Sciences

www.elsevier.com/locate/ijts

Nine-step phenomenological diesel soot model validated over a wide range of engine conditions

Feng Tao *, Rolf D. Reitz, David E. Foster, Yi Liu

Engine Research Center, University of Wisconsin–Madison, Madison, WI 53706, USA

ARTICLE INFO

Article history:
Received 25 December 2007
Received in revised form 27 August 2008
Accepted 27 August 2008
Available online 26 September 2008

Keywords:
Phenomenological soot model
Multi-dimensional simulation
Diesel engine combustion

ABSTRACT

A nine-step phenomenological soot model has been implemented into the KIVA-3V code for predicting soot formation and oxidation processes in diesel engines. The model involves nine generic steps, i.e., fuel pyrolysis, precursor species (including acetylene) formation and oxidation, soot particle inception, particle coagulation, surface growth and oxidation. The fuel pyrolysis process leads to acetylene formation and it is described by a single-step reaction. The particle inception occurs via a generic gas-phase precursor species, and the precursor is the product of an irreversible reaction from acetylene. The acetylene addition reaction contributes to soot surface growth. The particle coagulation affects both particle size and number density. The oxidation of soot particles includes two mechanisms—Nagle and Strickland-Constable's O_2 oxidation mechanism and Neoh et al.'s OH oxidation mechanism. The quasi-steady state assumption is applied to an H_2–O_2–CO system for calculating OH concentration. Both acetylene and precursor species have their own consumption paths, each of which is described by a single-step oxidation reaction.

Validations of the model have been conducted over a wide range of engine conditions from conventional to PCCI-like combustion. Two engine examples (a heavy-duty diesel engine and a light-duty diesel engine) are presented in this paper. The predictions are compared against measurements, and the applicability of the model to multi-dimensional diesel simulations is assessed. The model's capability of predicting the soot distribution structure in a conventional diesel flame is included in discussion as well. The work reveals that the nine-step model is not only computationally efficient but also fundamentally sound. The model can be applied to diesel engine combustion analysis and, after calibration, is suitable to be integrated with genetic algorithms for system optimization over a controllable range of operations.

1. Introduction

Over the past two decades between 1988 and 2008, the US Environmental Protection Agency (EPA) implemented three standards for on-highway heavy-duty diesel engine emissions. In the 1998 standards, a target for tailpipe particulate matter (PM) emissions was introduced and it was set at 0.1 g/bhp hr. This target was moderately stringent, only about a factor of 6 less than that of the 1988 standards (0.6 g/bhp hr). In the next standards mandated in 2004, the EPA revised its target for nitrogen oxides (NOx), but allowed the 1998 PM emissions target to be carried over. However, since the beginning of 2007, the EPA aggressively tightened its measures in the 2007 standards, introducing a new target that requires further reduction on PM emissions by an additional factor of 10 (i.e. 0.01 g/bhp hr), with simultaneous reduction on NOx emissions by an additional factor of 12.5 (i.e. 0.20 g/bhp hr).

In order to meet this ambitious PM target, today's diesel engines have inevitably adopted diesel particulate filter (DPF) after-treatment systems. Although the DPF systems can help to effectively reduce diesel tailpipe PM emissions well below the US EPA 2007 mandate, it is generally agreed that the use of DPFs is not an ultimate solution for diesel engines to meet forthcoming, even more stringent PM emissions standards. One of the reasons is that the regeneration of DPFs sets an upper limit on their conversion efficiency and lifespan. Besides, the after-treatment devices add additional cost to new vehicles and, most importantly, they cannot help to improve CO_2 emissions and fuel consumption.

For better solutions, modern diesel technologies take advantage of injection system improvement, engine geometry modification and even fuel/lubricant oil reformation, and researchers are pursuing methods that are able to optimize combustion systems and, in turn, minimize engine-out and/or tailpipe emissions. Examples of these methods include homogeneous charge compression ignition (HCCI), premixed charge compression ignition (PCCI), modulated kinetics (MK) combustion, and low-temperature combustion (LTC), etc. Unlike conventional diesel operation, these optimized combustion modes have demonstrated great potential of being able to simultaneously reduce NOx and PM emissions to levels acceptable

* Corresponding author. Fax: +1 (608) 262 6707.

1290-0729/$ – see front matter
doi:10.1016/j.ijthermalsci.2008.08.014

for future emissions regulations. If such combustion concepts can be realized in real engine operation, the conversion efficiency required for the DPF systems will be reduced significantly.

Conventional diesel operation refers to the processes that direct-injection (DI) diesel engines employ a single spray injection event and their in-cylinder combustion demonstrates a unique heat-release behavior. The heat release has two distinct phases: the premixed phase and the mixing-controlled phase. The premixed combustion phase is a result of fast, spontaneous reactions of the vapor-fuel and air mixture. It is characterized by a rapid rise in the apparent heat release rate, lasting only a few crank angle degrees after ignition. In the second phase, mixing between the fuel and the surrounding charge becomes a dominant factor that limits the rate of heat-release-controlling reactions, and the apparent heat release rate curve changes gradually over a relatively long crank angle period. Due to the existence of over-rich mixtures in regions surrounded by high-temperature stoichiometric burning, a considerable number of soot particles (or PMs) are formed in the mixing-controlled phase, though many of them are oxidized quickly on the high-temperature burning surfaces.

The soot formation processes in diesel engines involve rather sophisticated physics and chemistry. Nevertheless, the traditional approach adopted in multi-dimensional engine modeling is to use a high-temperature reaction model for soot formation. The model links the concentration of fuel vapor directly to soot, consisting merely of a lumped, single-step reaction with high activation energy. The formation rate of soot particles is expressed in the Arrhenius form by the equation proposed by Hiroyasu et al. [1]:

$$\left.\frac{dm_{\text{soot}}}{dt}\right|_{\text{form}} = A_f m_{\text{fuel}} p^{0.5} \exp\left(-\frac{E_f}{RT}\right) \tag{1}$$

where m_{soot}, m_{fuel}, p, T, and R are the soot mass, the fuel vapor mass, the pressure, the temperature, and the universal gas constant, respectively. The rate constant has an activation energy, E_f, with a value of 8×10^4 [J/mol], and a pre-exponential factor, A_f, that can be adjusted to ensure agreement between the calculated soot yields and the measured engine-out soot emissions. In engine simulations, this soot formation model is commonly employed in conjunction with the Nagle and Strickland-Constable soot oxidation model [2]. The combined model, called Hiroyasu's two-step soot model [1], has been very helpful in providing knowledge on bulk soot distribution and transport in the high-temperature combustion environments of conventional diesel engines (e.g., [3]).

Unfortunately, since Hiroyasu's model oversimplifies the diesel soot formation processes, only limited success exists so far, particularly when the soot formation process in the optimized combustion modes is the subject of studies. In optimized combustion modes, a variety of control strategies (e.g., very early injections, split/multiple injection pulses, high exhaust gas recirculation, reduced compression ratio, swirl, etc.) are introduced for achieving better mixture preparation and/or for reducing combustion temperature. Under such combustion environments, the low-temperature reaction channels dominate the soot formation processes, for which Hiroyasu's high-temperature soot formation model is not suitable anymore. It has been demonstrated that, in many cases (e.g., [4–6]), the predicted results are only partially and/or not fully in agreement with the trends of measured engine-out soot emissions.

In a recent work [7,8], three different soot modeling approaches were compared and several advantages of multi-step phenomenological (MSP) soot models highlighted. First, the MSP soot models involve only a few more steps than the two-step soot model, thus introducing almost no extra cost in computations. Second, the models distinguish the soot formation processes by two major reaction steps: one for particle inception and the other for surface growth. This approach allows the soot formation step to be separated into two reactions with different activation energies, with which both high-temperature and low-temperature formation regimes might possibly be covered. Moreover, the models are obviously advantageous because they include particle dynamics, being able to predict the sizes and the number density of soot particles formed in engines. Given the speculation that the forthcoming emissions regulation will soon impose a measure on the number and size of tailpipe PMs, the MSP modeling approach continues to receive renewed attention (e.g., [9]).

To demonstrate the utility of multi-step phenomenological soot models, a previously developed MSP model [10,11] was revised and applied to the modeling study of low-temperature soot formation processes [12]. The study was based on a light-duty HSDI diesel engine with a displacement of 422 cm^3/cylinder and a compression ratio of 18.7, being operated at a low fueling load (IMEP = 3 bar). An EGR sweep ranging from 0% to 68% was investigated. The simulations showed that the prediction was able to reproduce the trend of engine-out soot emissions. When the EGR rate is increased, the soot emissions level increases; nevertheless, when the EGR rate exceeds a critical value (over 60% in the study), the soot emissions decrease while the EGR continues to increase. This prediction agrees the observation reported by Akihama et al. [13].

In a parallel study [14], the same approach was adopted in the simulations for a production HSDI diesel engine with optimal engine performance. The engine was operated using split injection that had a small pilot injection (5% of total fuel mass) and a main injection with an injection dwell of 19 °CA. Six cases of different injection timings ranging from −18.5 to −28.5 °CA ATDC were simulated. The results predicted using Hiroyasu's two-step model and two MSP soot models were compared to each other as well as to measurements. The comparison demonstrated that the revised MSP soot model made considerable improvement to the predictions of soot emissions generated from this production HSDI diesel engine.

All engine simulations [12,14] mentioned above employed a modified KIVA-3V code [15] in which the "Shell" ignition model and the characteristics time combustion (CTC) model [16] were implemented. In order to improve the model fidelity but maintain the simplicity of ignition and combustion sub-models, a quasi-steady state H_2–O_2–CO system [17] was introduced into the nine-step soot model. The H_2–O_2–CO system was proposed to handle problems associated with the calculations of OH concentrations. The OH radical is a critical species to both NO formation and soot oxidation processes. Nevertheless, in the previous work [12,14], the OH concentrations were calculated using the concept of chemical equilibrium, the assumption of which was unfortunately unrealistic when applied to transient diesel combustion processes. The updated nine-step soot model was successfully applied to analyze the soot distribution structure in a conventional diesel flame for a benchmark (Cummins) heavy-duty diesel engine case [17,18], based on which a comparison to the two-step soot model was attempted.

In this paper, effort on extensive validations of the updated nine-step phenomenological soot model over a wide range of engine conditions is reported. The objective of the work is to assess to what extent the model can be applied to multi-dimensional simulations for prediction of soot particle emissions in diesel engines. In the following sections, the updated nine-step soot model is described firstly in detail. Then, the simulated results of two diesel engines (a heavy-duty diesel engine and a light-duty diesel engine) operated at both conventional and PCCI-like conditions are illustrated with comparison to measurements. Finally, the model's capabilities for engine soot modeling will be discussed and assessed. It is expected that the documentation can be used as a reference for researchers who work with diesel engine combustion analysis and system optimization.

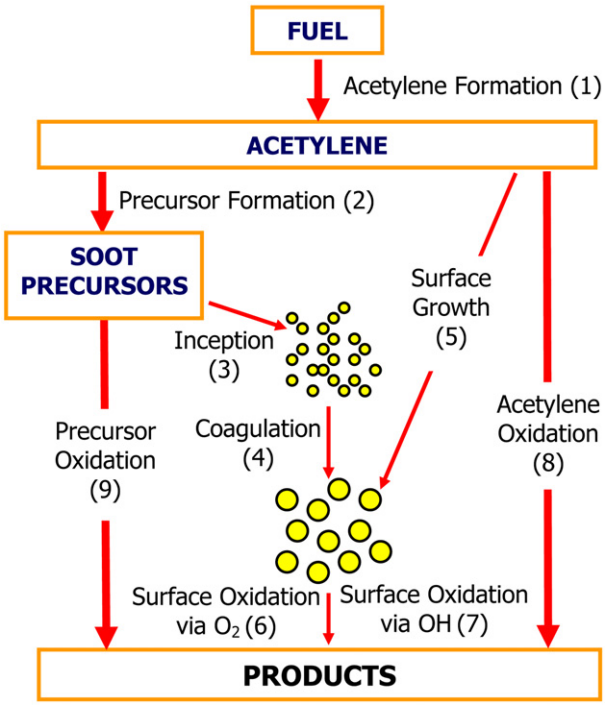

Fig. 1. Schematic of the nine-step phenomenological diesel soot model.

2. Phenomenological soot model

The schematic representation in Fig. 1 [12,14,17] shows the structure of the nine-step phenomenological soot model. The model retains the main features of the original model [10,11] but contains three major modifications: (1) fuel pyrolysis leads solely to acetylene formation; (2) the soot precursor is formed merely via acetylene (i.e., not directly from fuel); (3) an OH-related soot oxidation step is added. Besides, an H_2–O_2–CO system is introduced for calculating the OH concentration [17]. These modifications make the model consistent with the complex-chemistry coupled phenomenological soot model [19], but it is more suitable to be coupled with the "Shell" ignition model and the characteristic time combustion (CTC) model [16] for computationally efficient, multi-dimensional diesel combustion simulations. Due to change in the model structure, the rate constants of some steps have to be adjusted or proposed.

The revised phenomenological soot model involves nine steps. A detailed description of the model is given below.

STEP 1: Acetylene (C_2H_2) formation

$$\text{Fuel} \xrightarrow{\dot{R}_1} \frac{m}{2}C_2H_2\text{:}\quad \dot{R}_1 = \frac{m}{2}k_1[\text{Fuel}] \tag{2}$$

where $k_1 = 1.0 \times 10^{10}\exp(-2.5 \times 10^4/T)$ (s^{-1}) and it is higher than the rate constant proposed by Fusco et al. [10] by two orders of magnitude. m denotes the number of carbon atoms in the fuel and [ ] indicates the molar concentration (mole cm^{-3}). In the current model, m is assigned to be 14, since the fuel is modeled as $C_{14}H_{30}$.

STEP 2: Precursor species (R) formation

$$C_2H_2 \xrightarrow{\dot{R}_2} \frac{2}{z}R + H_2\text{:}\quad \dot{R}_2 = \frac{2}{z}k_2[C_2H_2] \tag{3}$$

where $k_2 = 1.0 \times 10^{11}\exp(-2.0 \times 10^4/T)$ (s^{-1}) is proposed for the precursor formation, and z denotes the number of carbon atoms in the precursor species. The generic precursor species is assumed to be of fullerene type, consisting of 60 carbon atoms, i.e., $z = 60$.

STEP 3: Particle inception

$$R \xrightarrow{\dot{R}_3} P\text{:}\quad \dot{R}_3 = zk_3[R] \tag{4}$$

where $k_3 = 5.0 \times 10^7\exp(-2.52 \times 10^4/T)$ (C-atom $mole^{-1}$ cm^3 s^{-1}). The rate constant is reduced from the original constant of Fusco et al. [10] by a factor of 5.0×10^{-3}.

Soot particles are assumed to be dry, graphite-like particles containing solely carbon atoms. Strictly speaking, this assumption is incorrect, particularly for young soot particles that contain significant amount of hydrogen. Nevertheless, this assumption is accepted in the absence of other better alternatives. The incipient soot particles are assumed to have a diameter of 1.28 nm, which corresponds to about 100 carbon atoms. There exist many other theories, some of which assume the nucleation size to be 25 nm, for example, in Fusco's model [10,11].

STEP 4: Particle coagulation

$$xP \xrightarrow{\dot{R}_3} P\text{:}\quad \dot{R}_4 = \frac{1}{2}k_4N^2 \tag{5}$$

where k_4 is the collision frequency constant, valid for regimes ranging from the free-molecular regime to the near-continuum regime [11]. x ($x \geqslant 2$) indicates symbolically the number of particles that participate in the coagulation processes. In the calculation, the coagulation rate is proportional to N^2, where N is the soot number density.

Since the gas mean free path is comparable with the particle size in high-pressure diesel combustion environments, Kazakov and Foster [11] employed a collision frequency constant defined as

$$k_4 = \frac{k_{fm}k_{nc}}{k_{fm} + k_{nc}} \tag{6}$$

The free-molecular collision frequency for the equally-sized particles, k_{fm}, is given by

$$k_{fm} = 4\alpha\sqrt{\frac{6k_BTd_p}{\rho_s}} \tag{7}$$

where α is the van der Waals enhancement factor, assumed equal to 2, k_B is the Boltzmann constant, ρ_s is the density of soot particle, assumed equal to 2 g/cm^3, and

$$d_p = \left(\frac{6M_Cy_s}{\pi N\rho_s}\right)^{1/3} \tag{8}$$

the diameter of soot particle. In Eq. (8), M_C and y_s are the molecular weight of a carbon atom (12 g/mol) and the molar concentration of soot, respectively.

The near-continuum coagulation constant, k_{nc}, is defined as

$$k_{nc} = \frac{8k_BT}{\mu}(1 + 1.257Kn) \tag{9}$$

where μ is the molecular viscosity of the gas, $Kn = 2\ell/d_p$ the Knudsen number, and ℓ is the gas mean free path. The factor of 1.257 represents the near-continuum slip correction factor.

STEP 5: Surface growth

$$P + C_2H_2 \xrightarrow{\dot{R}_5} P + H_2\text{:}\quad \dot{R}_5 = k_5[C_2H_2](A_{\text{Soot}})^{1/2} \tag{10}$$

where $k_5 = 1.05 \times 10^4\exp(-3.1 \times 10^3/T)$ (cm^{-1} s^{-1}) and A_{Soot} represents the total surface area of soot particles (cm^2), which are assumed to be spherical. Here, the rate of surface growth is assumed to be proportional to $(A_{\text{Soot}})^{1/2}$, as suggested by Leung et

al. [20]. The current rate constant, k_5, has been modified according to the calibration of the present study.

STEP 6: O_2-related surface oxidation

$$P + O_{20} \xrightarrow{\dot{R}_6} P + 2CO:\ \dot{R}_6 = k_6 A_{Soot} \tag{11}$$

where the oxidation rate constant k_6 is the NSC oxidation model constant [2].

The *NSC* oxidation reactions are semi-empirical, involving two reaction sites on the surface of a soot particle: (1) significantly more reactive sites A; and (2) less reactive sites B. The fraction of the surface site A is denoted by x_A, and the remaining fraction $1 - x_A$ is for the surface site B. The *NSC* reaction scheme can be described as follows:

$$A_{site} + O_2(g) \xrightarrow{k_A} \text{Surface oxide:}$$

$$k_A = 20\exp(-15100/T)\ [\mathrm{g/cm^2\,s\,atm}] \tag{12a}$$

$$\text{Surface oxide} \xrightarrow{k_A/k_Z} 2CO(g) + A_{site}:$$

$$k_Z = 21.3\exp(2060/T)\ [\mathrm{atm^{-1}}] \tag{12b}$$

$$B_{site} + O_2(g) \xrightarrow{k_B} 2CO(g) + A_{site}:$$

$$k_B = 4.46 \times 10^{-3}\exp(-7640/T)\ [\mathrm{g/cm^2\,s\,atm}] \tag{12c}$$

$$A_{site} \xrightarrow{k_T} B_{site}:$$

$$k_T = 1.51 \times 10^{5}\exp(-48800/T)\ [\mathrm{g/cm^2\,s}] \tag{12d}$$

The *NSC* oxidation rate (units of mole C-atom/cm^2 s) is given by:

$$k_6 = \left[\left(\frac{k_A p_{O2}}{1 + k_Z p_{O2}}\right)x_A + k_B p_{O2}(1 - x_A)\right] \tag{13}$$

where the fraction x_A can be calculated by the steady-state assumption of site A formation:

$$x_A = (1 + k_T/k_B p_{O2})^{-1} \tag{14}$$

STEP 7: OH-related surface oxidation

$$P + OH \xrightarrow{\dot{R}_7} P + CO + \frac{1}{2}H_2:\ \dot{R}_7 = k_7 A_{Soot} \tag{15}$$

where the oxidation rate constant k_7 is taken from Neoh et al. [21]. Unlike the approach adopted in previous work [12,14], the concentration of OH radical is estimated from a H_2–O_2–CO_2 system (Table 1) in the current work. The OH concentration is derived by applying the quasi-steady state assumption, i.e.,

$$\frac{d[OH]}{dt} = 0 \tag{16}$$

which leads to

$$[OH] = \frac{k_1^+[H][O_2] + k_2^+[O][H_2] + k_3^-[H_2O][H]}{k_1^-[O] + k_2^-[H] + k_3^+[H_2] + k_4^-[OH] + k_5^-[H][M] + k_6^+[CO]} + \frac{k_4^+[O][H_2O] + k_5^+[H_2O][M] + k_6^-[CO_2][H]}{k_1^-[O] + k_2^-[H] + k_3^+[H_2] + k_4^-[OH] + k_5^-[H][M] + k_6^+[CO]} \tag{17}$$

where k_i^+ and k_i^- are the forward and backward reaction rate constants of each reaction i ($i = 1, 6$), respectively, and they satisfy $k_{eq,i} = k_i^+/k_i^-$, in which $k_{eq,i}$ is the equilibrium constant of each reaction i. M indicates the third-body species, $[M] = P/RT$. The concentrations of O and H are obtained using the chemical equilibrium calculation of $O_2 \Leftrightarrow 2O$ and $H_2 \Leftrightarrow 2H$, respectively.

STEP 8: Acetylene oxidation

$$C_2H_2 + O_2 \xrightarrow{\dot{R}_8} 2CO + H_2:\ \dot{R}_8 = k_8[C_2H_2][O_2] \tag{18}$$

Table 1
The H_2–O_2–CO_2 system used for the quasi-steady state OH calculation

No.	Reactions	K_f		
		A	b	E (cal/mole)
1	$H + O_2 \Leftrightarrow O + OH$	1.915e14	0.00	1.644e04
2	$O + H_2 \Leftrightarrow OH + H$	5.080e04	2.67	6.292e03
3	$OH + H_2 \Leftrightarrow H_2O + H$	2.160e08	1.51	3.430e03
4	$O + H_2O \Leftrightarrow OH + OH$	2.970e06	2.02	1.340e04
5	$H_2O + M \Leftrightarrow H + OH + M$	1.912e23	−1.83	1.185e05
6	$CO + OH \Leftrightarrow CO_2 + H$	9.430e03	2.25	−2.351e03

where $k_8 = 6.0 \times 10^{12}\exp(-2.52 \times 10^4/T)$ ($\mathrm{mole^{-1}\,cm^3\,s^{-1}}$). This constant is an order of magnitude less than Fusco's rate constant.

STEP 9: Precursor species (R) oxidation

$$R + OH \xrightarrow{\dot{R}_9} CO + \frac{1}{2}H_2:\ \dot{R}_9 = k_9[R][OH] \tag{19}$$

where $k_9 = 1.0 \times 10^9\exp(-2.0 \times 10^4/T)$ ($\mathrm{mole^{-1}\,cm^3\,s^{-1}}$). The original Fusco's model constant is reduced by an order of three in magnitude.

Steps 1, 2, 8, and 9 are global expressions for the gas-phase reactions, whereas Steps 3, 4, 5, 6, and 7 describe particle-related reactions. The net rates of formation for the soot mass density, Y_S, and the soot number density, N, can be written as

$$\frac{d}{dt}(Y_S) = M_C(\dot{R}_3 + \dot{R}_5 - \dot{R}_6 - \dot{R}_7) \tag{20}$$

$$\frac{d}{dt}\left(\frac{N}{N_A}\right) = \frac{M_C}{M_{nuc}}\dot{R}_3 - \dot{R}_4 \tag{21}$$

where N_A and M_{nuc} are Avogadro's number and the weight of a particle nucleus, respectively.

These two equations involve the kinetic reaction rates of the soot formation, coagulation and oxidation processes, which can be strongly affected by turbulent mixing. To account for the turbulence-chemistry interaction, the rates in Eqs. (20) and (21) are modified using a correlation factor that combines chemical and turbulent time scales:

$$\dot{R}_i' = \frac{\tau_{ch,i}}{\tau_{ch,i} + \tau_{mix}}\dot{R}_i, \qquad \tau_{mix} = c\frac{k}{\varepsilon} \tag{22}$$

where $\tau_{ch,i}$ is the chemical time scale of each step. τ_{mix} is the mixing time scale, k the turbulent kinetic energy, ε the turbulent dissipation rate, c has a value of 0.25.

3. Numerical methodology

The CFD code used in the simulations is a modified version of the KIVA-3V code [15]. Several physics and chemistry sub-models developed at Engine Research Center (ERC), University of Wisconsin–Madison have been implemented in the code. These sub-models include the "Shell" model for ignition [16], the laminar-and-turbulent characteristic time combustion (CTC) model for post-ignition combustion [16], the Zel'dovich model for NO formation, the RNG k–ε model for low Mach-number turbulent flow modeling [22], a 'blob' injection model for fuel parcel injection [23], a surface wave model involving the Kelvin–Helmholtz model [24,25] and the Rayleigh–Taylor model [26] for spray atomization and droplet breakup, a droplet wall impingement model, a crevice model for piston-ring flow, and a modified wall heat transfer model [27]. The nine-step phenomenological diesel soot model described in the preceding section has been implemented into the ERC KIVA-3V code for modeling soot formation and oxidation processes in engines as well.

Table 2
Caterpillar heavy-duty engine specifications and operating conditions

Engine	Caterpillar 3401E SCOTE
Bore	137.2 mm
Stroke	165.1 mm
Compression ratio	16.1:1
Displacement	2.44 Liters
Connecting rod length	261.6 mm
Squish height	1.57 mm
Combustion chamber geometry	In-Piston Mexican Hat with Sharp Edged Crater
Piston	Articulated
Charge mixture motion	Quiescent
Maximum injection pressure	190 MPa
Injector type	A production style Caterpillar electronic unit injector (EUI)
Number of nozzle holes	6
Nozzle hole diameter	0.214 mm
Spray angle	130°
Start of injection (SOI)	−20, −15, −10, −5, 0, 5 °CA ATDC (see Table 3)
Engine speed	821 rev/min
Intake manifold temperature	313 K
EGR	8, 27, 40% (see Table 3)
Load	25%

Table 3
Experimental conditions (25% load and 821 rev/min) of Caterpillar diesel engine

Cases		SOI (ATDC)	EGR (%)	NOx (g/kg f)	Soot (g/kg f)	BSFC (g/kW hr)	Merit
EGR = 8%	A1	−20	6.41	149.4	0.176	244	80
	A2	−15	6.39	104.9	0.138	224	197
	A3	−10	7.79	64.1	0.188	218	411
	A4	−5	8.83	41.0	0.329	216	608
	A5	0	9.39	25.4	0.444	223	712
	A6	+5	10.40	25.1	0.234	231	687
EGR = 27%	B1	−20	26.83	78.0	0.474	230	274
	B2	−15	27.29	40.4	0.388	219	596
	B3	−10	27.39	20.3	0.302	212	829
	B4	−5	28.04	12.0	1.041	218	736
	B5	0	28.13	8.2	1.112	223	707
	B6	+5	28.19	9.7	0.435	232	796
EGR = 40%	C1	−20	40.00	30.0	0.291	227	662
	C2	−15	40.00	14.6	0.509	218	821
	C3	−10	40.00	6.8	0.795	219	805
	C4	−5	40.00	4.0	1.373	217	685
	C5	0	40.00	3.1	1.157	223	709
	C6	+5	40.00	2.5	0.612	245	739

All the simulations were performed using sector meshes of engines, in which only one single spray was involved. Each computation started from IVC (intake valve closure) and ended at EVO (exhaust valve opening). All the input conditions were calculated using a 1-D cycle simulation code [28] that accounts for gas exchange processes in the intake manifold including EGR. As the diesel ignition process was described by the "Shell" ignition model, the constant, af04, was adjusted first to ensure the ignition timing in the baseline cases in agreement with measurements. For the other cases, the same value of af04 applied.

4. Heavy-duty diesel engine

The heavy-duty diesel engine chosen as an example for illustration is a Caterpillar 3400 series, single-cylinder oil test engine (SCOTE). The experiments [29] were conducted to achieve optimal operation with low fuel consumption and engine-out emissions (NOx and PMs). In order to automate engine operations, the genetic algorithm (GA) optimization methodology was applied to the experiments. A merit function, served as the objective function of the GA optimization, was defined as

$$\text{Merit} = \frac{1000}{(\frac{\text{BSFC}}{\text{BSFC}_0}) + (\frac{\text{NOx}}{\text{NOx}_0})^2 + (\frac{\text{PM}}{\text{PM}_0})^2} \tag{23}$$

where the index 0 indicates the target values. For NOx and PMs, the targets were 80% of the US EPA 2004 mandate, i.e., 2.682 and 0.107 g/kW hr, respectively. The BSFC target was 200 g/kW hr, which was about 40% efficiency of the current load conditions.

During the engine experiments [29], a production Caterpillar electronic unit injector (EUI) was used for fuel injection, and the parameters such as intake pressure, start of injection (SOI) and EGR were varied. The engine is installed at the ERC laboratories, and its specifications and operating conditions are listed in Table 2.

Eighteen tests were selected as the representative cases of the heavy-duty diesel engine. These experimental cases cover a wide range of SOI timing and EGR. The SOI timings were varied from −20 to 5 °CA ATDC, and the EGR were supplied at three levels (i.e., 8, 27, and 40%). The engine was operated at Mode 2, corresponding to 25% load and 821 rev/min. The temperature of the intake charge (including both EGR and fresh air) was maintained at 313 K. The test matrix is provided in Table 3.

Three cases (A3, B3, C3 in Table 3), which correspond to SOI = −10 °CA ATDC, were selected as the baseline cases. As the "Shell" ignition model is insensitive to variations in EGR (e.g., [12]), the constant af04 has to be tuned to ensure the matching of ignition timing. The values of 1.75e5, 1.55e5 and 1.20e5 were found to be suitable for af04 for three baseline cases of different EGR ratios, i.e., 8, 27 and 40%, respectively. The same value of af04 was applied to the other cases at the same EGR level in the simulations.

In Fig. 2, the predicted in-cylinder pressures and heat release rates are compared to measurements. Only three cases of different SOI timings (−20, −10, and 5 °CA ATDC) and EGR = 8% are illustrated. The overall predictions of these three cases are acceptable, particularly for the baseline case (i.e., SOI = −10 °CA ATDC). For the other two cases, the predicted ignition timings are slightly longer than measurements but the combustion strengths are reasonably reproduced. For other EGR ratios (i.e., 27 and 40%), similar performance on the in-cylinder pressures and heat release rates can be observed.

The yields of total NOx and soot are shown in Fig. 3. As illustrated in the figure, the NOx increases after ignition, reaching high-level plateaus shortly and lasting until EVO. The engine-out NOx is the highest for the case of EGR = 8% whereas for the case of EGR = 40% the lowest. This observation is in agreement with the general expectation. It is known that EGR has a strong effect on combustion temperature: the higher the EGR ratio, the lower the combustion temperature; a higher EGR ratio leads to lower engine-out NOx.

As Fig. 3 demonstrates, the soot formation dominates in the beginning, which leads to a quick buildup of total soot mass; in the second period, the soot oxidation gains strength and the soot yield declines to the engine-out level within a period of about 60 crank angle degrees. The peak of the soot yield predicted is about 100 times higher than the engine-out soot.

For the case of higher EGR (40%), the peak soot yield is relatively lower but the engine-out value is higher. The ratio between the peak and the engine-out soot reduces with increase in EGR. This result is not difficult to understand: the in-cylinder temperature is relatively lower at higher EGR conditions, which corresponds to slower soot formation rate and reduced soot oxidation strength.

Fig. 4 compares the predicted engine-out NOx to measurements. It is shown in the figure that the predictions are in agreement with the measurements, particularly for the cases in which SOI is not earlier than −10 °CA ATDC. For the earlier injection cases (EGR = 8 and 27%), the predicted engine-out NOx are relatively higher than experiments. The combination of the H_2–O_2–CO_2 sys-

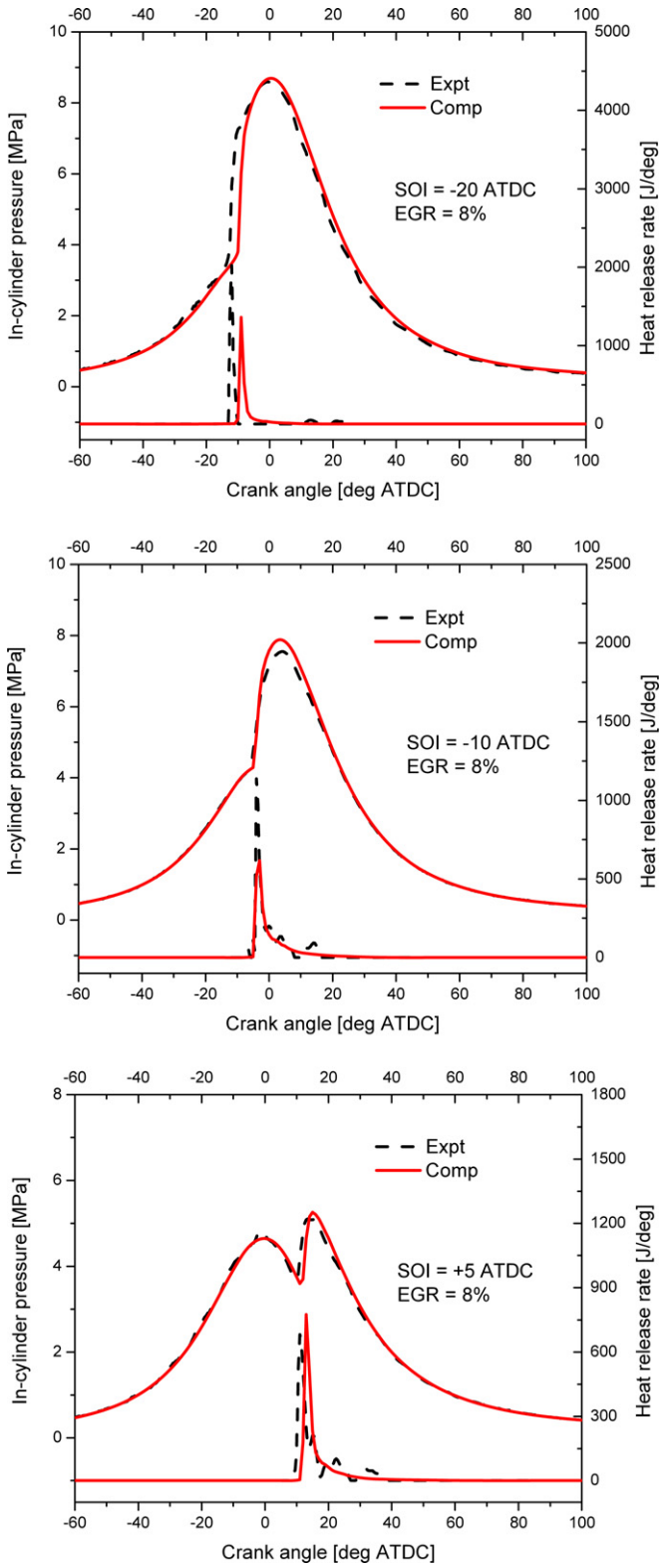

Fig. 2. Comparison of predicted and measured in-cylinder pressures and heat release rates for three cases of Caterpillar heavy-duty diesel engine: SOI = −20, −10, and 5 °CA ATDC (A1, A3, A6 in Table 3) and 8% EGR.

tem and the CTC model might lead to predict an unrealistically higher OH yield, and thus higher NOx production. The other reason could be that the prolonged ignition delay (see Fig. 2) allows excessive fuel to be evaporated, therefore resulting in rapid premixed combustion and higher combustion temperatures.

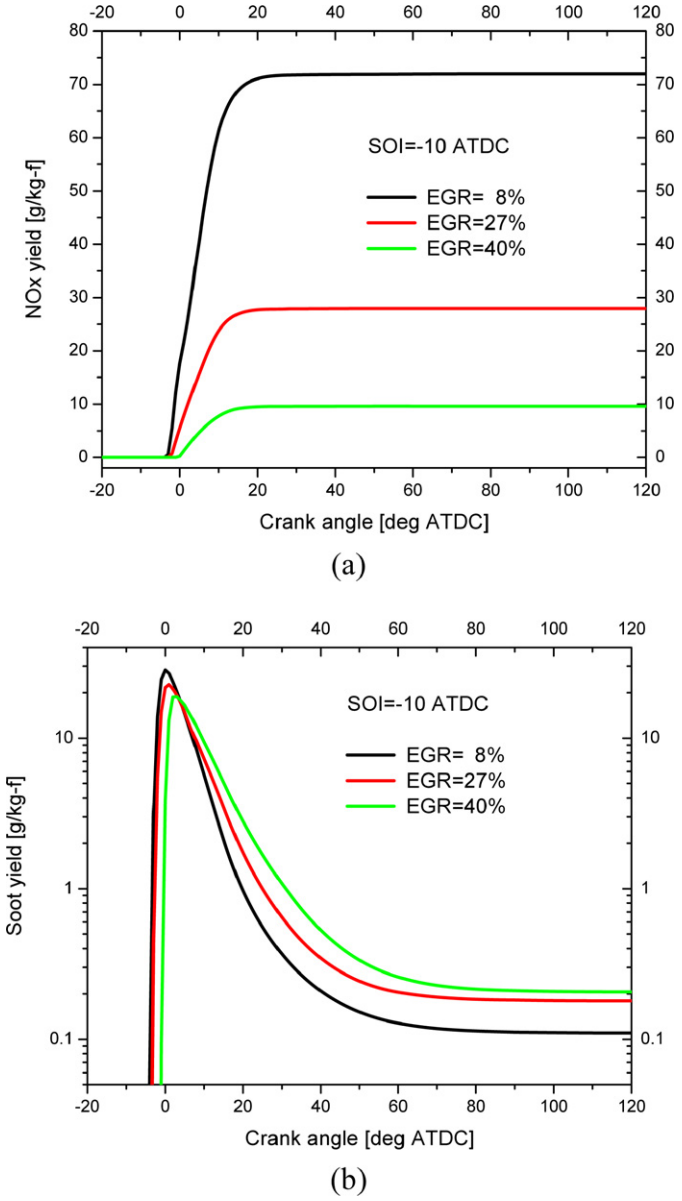

Fig. 3. Total yields of NOx and soot predicted for three cases of Caterpillar heavy-duty diesel engine: EGR = 8, 27, and 40% and SOI = −10 °CA ATDC (A3, B3, and C3 in Table 3).

Comparisons between the predicted and measured engine-out soot emissions are illustrated in Fig. 5. For the 8% EGR cases, the predicted results match reasonably well with the measurements both in trend and in quantity. For the 27% EGR cases, the trend of the predicted soot agrees with the measurements, though a correction factor of two is needed to ensure the magnitude of predictions in agreement with that of the measured data. For the 40% EGR cases, a correction factor of three is desired if the rate constants of the soot model remain unchanged.

The discrepancies shown in Fig. 5 can be a result of several sources, for example, due to different chemical natures in the predicted soot and in the measured PMs. The soot model assumes soot particles to be dry, graphite-like particles containing merely carbon atoms, whereas the measured PMs contain a certain fraction of soluble organic compounds (SOCs).

It must be pointed out that all the simulations mentioned above were exercised using the same rate constants of the soot model [17]. Since the soot model was implemented into the KIVA-3V code of an ERC version, in which the “Shell” ignition model

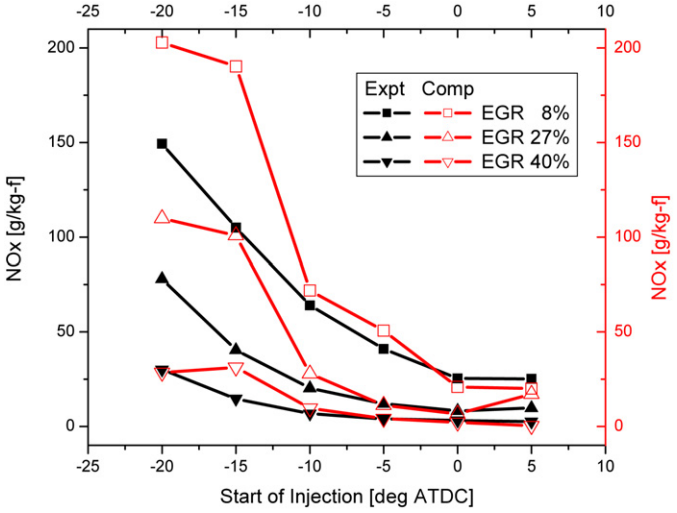

Fig. 4. Comparison of predicted engine-out NOx and measured NOx emissions for Caterpillar heavy-duty diesel engine.

and the CTC model were involved, it was not unexpected to see some discrepancies when these sub-models were applied all together to a wide range of operating conditions particularly at high EGR ratios. These simple sub-models, often favored by industry researchers, can lead to computationally efficient solutions. On the other hand, compared to the results predicted using a comprehensive soot model (see, Table 8 in [30]), the nine-step soot model appears to be not only comparable, in terms of its predictability, but also competitive, in terms of its applicability for diesel combustion analysis and system optimization.

It should be reiterated that the objective of this work was not to calibrate the model constants but to exercise the existing, updated nine-step soot model [17,18], based on which the model would be assessed. Following this principle, the discrepancies illustrated in Fig. 5 should be considered acceptable, but not unexpected, not to mention the possibility of adjusting the model rate constants over a controllable range of operations particularly different EGR ratios.

5. Light-duty diesel engine

The same engine used in the previous study [14] was chosen as a representative example for light-duty diesel engines. It is a single-cylinder version of a 2.4-Liter, five-cylinder HSDI production diesel engine, and it can produce power up to 21 kW at 4200 rev/min. A series of tests over a range of swirl ratios, injection timings, and EGR ratios were conducted to optimize the engine performance with split injections at a single engine operating condition, i.e., 1757 rev/min and 45% load [31]. The optimal engine performance with split injection was achieved with an injection pressure of 110 MPa, an EGR ratio of 26.7%, an injection dwell of 19 °CA, and a pilot injection duration (energizing time) ETp of 90 μs. The optimal split injection profile measured in experiments is shown in Fig. 6, with SOI of −18.5 °CA ATDC. It has a pilot injection of small quantity (5% of total fuel mass), followed by a main injection.

The fuel used in the tests was #2 diesel obtained from a commercial fuel vendor. The injection system was a prototype Fiat/Bosch common-rail injection system, being capable of a maximum injection pressure up to 135 MPa. The injection system used in the experiments was an electro-hydraulically controlled unit injection system. The specifications of the engine and the common-rail injection system are summarized in Table 4.

Six of these tests [31], typical of split injection in light-duty diesel engines, were selected for presentation. Like the previ-

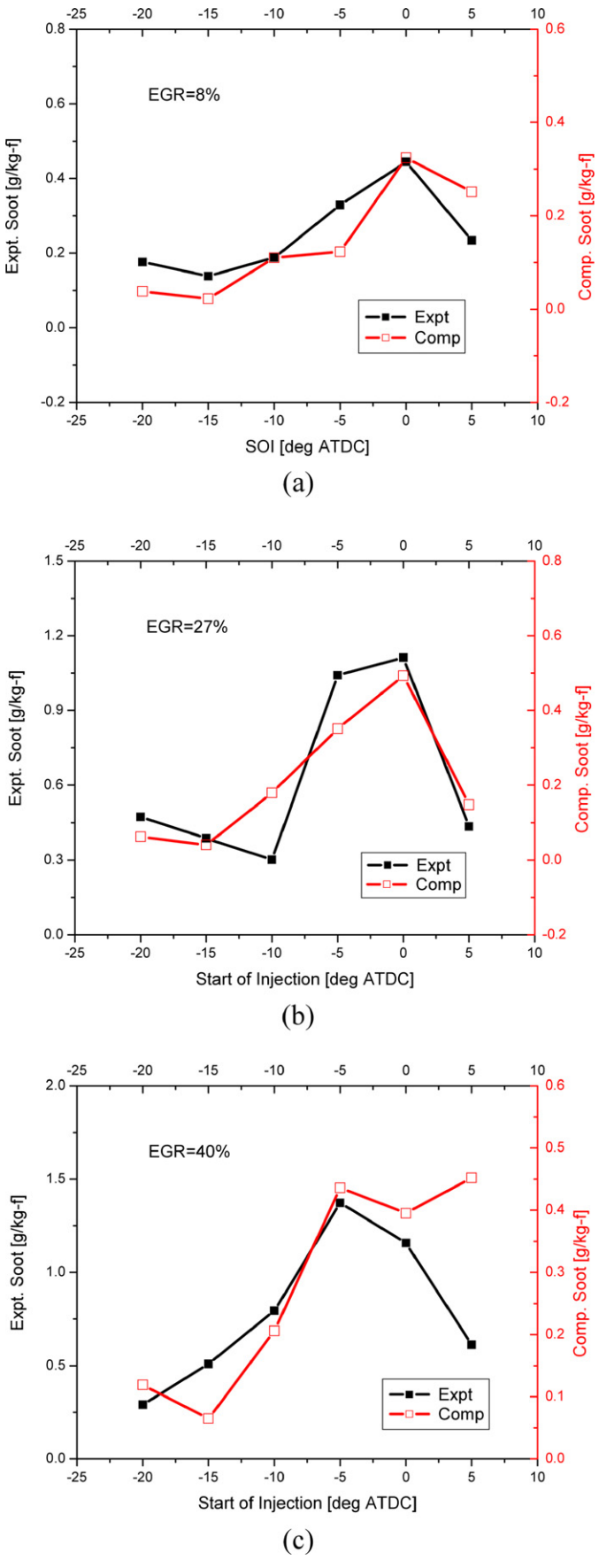

Fig. 5. Comparison of predicted engine-out soot and measured soot emissions for Caterpillar heavy-duty diesel engine: (a) 8% EGR; (b) 27% EGR; (c) 40% EGR.

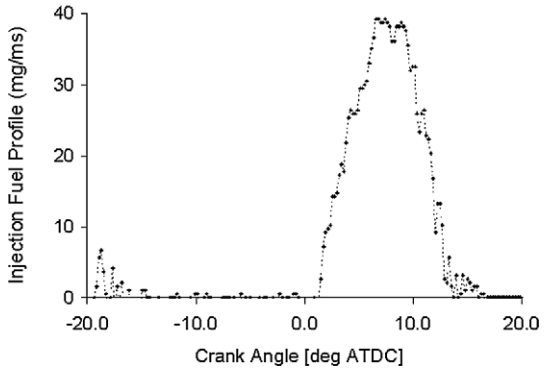

Fig. 6. Optimal split injection profile used for experiments of light-duty diesel engine.

Table 4
Light-duty engine and injector specifications and operating conditions

Engine	Single-cylinder, DI diesel
Bore	82.0 mm
Stroke	92.4 mm
Compression ratio	18.79:1
Displacement	0.48 Liters
Piston	Reentrant bowl
Injector type	Electro-hydraulically controlled injector
Maximum injection pressure	135 MPa
Nozzle type	Dual guided VCO nozzle
Number of nozzle holes	6
Hole diameter	160 μm
Hole L/D ratio	6.25
Included spray angle	145°
Intake valve closing (IVC)	−142 °CA ATDC
Exhaust valve opening (EVO)	142 °CA ATDC
Start of injection (SOI)	−28, −26, −24, −22, −20, −18 °CA ATDC
Engine speed	1757 rev/min
EGR	∼27%
Load	45%

ous work [14], the present study focused on the SOI timing sweep tests. The six simulated cases employed the same injection rate profile (see Fig. 6), with different SOI timings ranging from −18.5 °CA ATDC to −28.5 °CA ATDC.

Comparison on the in-cylinder pressures and heat release rates between the predictions and measurements is shown in Fig. 7. The case of SOI = −18 °CA ATDC was treated as the baseline case and the ignition parameter af04 was tuned to achieve matching of the pilot and main ignition delay timings. The ignition delay and combustion phasing of the main injection were properly reproduced for the other five cases, whereas the pilot ignition timings were not. The discrepancy on the pilot ignition timings might be caused by the limitation of the "Shell" ignition model. On the other hand, using the same injection rate profile for all six cases might possibly not be a proper practice as well. In real operations, the fuel distributions and injection timings of both pilot and main injections could vary slightly for each of these six tests.

Fig. 8 compares the predicted engine-out NOx and soot to measured emissions data. During these simulations, the updated nine-step soot model [17,18] was employed without modification of rate constants. Fig. 8(a) demonstrates that the trend of the predicted engine-out NOx versus SOI is consistent with measurements. The best matching is for the case of SOI = −22 °CA ATDC, whereas the largest discrepancy exists for the case of SOI = −28 °CA ATDC. For the former, the prolonged pilot ignition delay compensates the strength of the main combustion, characterized by two main peaks in the measured heat release rate curves, thus leading to numerically proper prediction. For the case with SOI = −28 °CA ATDC, the improperly predicted long ignition delay of the pilot fuel adds excessive combustion strength into the main combustion phase, resulting in higher combustion temperature and over-predicted engine-out NOx. Although the best matching on the in-cylinder pressure and heat release rate is for the case of SOI = −18 °CA ATDC, the engine-out NOx is nevertheless slightly under-predicted. As shown in Fig. 7(a), one of the main heat release peaks is not able to be reproduced, reducing the main combustion intensity, which might contribute to the NOx under-prediction.

The predicted engine-out soot, plotted against SOI, agrees with measurements in trend (see Fig. 8(b)), though the magnitudes of predicted soot are higher marginally by a factor of 2. The discrepancy might be the results of imperfect prediction in the main combustion strength and a reduced strength in soot oxidation. The limitations of the "Shell" ignition model, the CTC model, the H_2–O_2–CO_2 system and other sub-models restrict the accuracy of OH-radical prediction, causing unbalanced trade-off in OH concentration between NO formation and soot oxidation. Once again, it should be emphasized that the goal of this exercise was not to calibrate the nine-step soot model updated in [17,18] for specific engines and operating conditions but to compare and assess the model performance over different engine and operating conditions. Taking all the uncertainties involved in engine measurements into consideration, it is therefore understandable to observe certain discrepancies associated with such predictions as shown in Fig. 8(b). A deviation by a factor of 2 is often considered acceptable, and even "accurate", in many engine applications. In other words, tuning the rate constants of the soot model should not be a difficult task practically, if the deviation factor is in a range of 2–3.

6. Discussion

The soot model described in this paper is an updated nine-step phenomenological soot model, which was proposed for investigating the soot particle distribution structure in a conventional, mixing-controlled diesel flame [17,18]. The investigation was conducted by means of simulations based on the conditions of a benchmark experiment that was performed on a Cummins, heavy-duty DI diesel engine [32]. The engine operation corresponded to a conventional diesel combustion mode, and a detailed description was provided in the previous publication [17]. Since the experiment reproduced the operating conditions of similar experimental studies conducted in an optically-accessible engine of same class at the Sandia National Laboratories, Dec's conceptual diesel soot model [33] was able to be used for comparison.

As shown by the temperature and soot distributions in the publications [17,18], the predicted mixing-controlled flame features a lifted, non-premixed flame, with a soot distribution structure in agreement with Dec's conceptual model [33]. Following the direction of spray injection, the early soot particles are formed upstream in the region where the fuel-rich premixed combustion occurs (a little downstream from the spray tip). Moving downstream, the soot concentration increases to its highest level in the interior zone (the "head vortex") near the leading edge of the flame. From the interior soot zone outwards, the concentrations of soot particles decrease gradually, reaching near-zero levels on the periphery of the flame due to oxidation.

The agreement in both flame and soot distribution structures not only reinforces the conceptual model [33], but also implies that the nine-step phenomenological soot model is fundamentally consistent with the basic physics and chemistry of diesel soot formation and oxidation processes. Moreover, extensive validations over a wide range of engine conditions reported in this paper confirm that the model is applicable to multi-dimensional simulations for diesel engine combustion analysis and, after proper calibration, to be integrated with genetic algorithms for system optimization.

So far, only validations based on the mass-based emissions data have been presented by means of two representative engine ex-

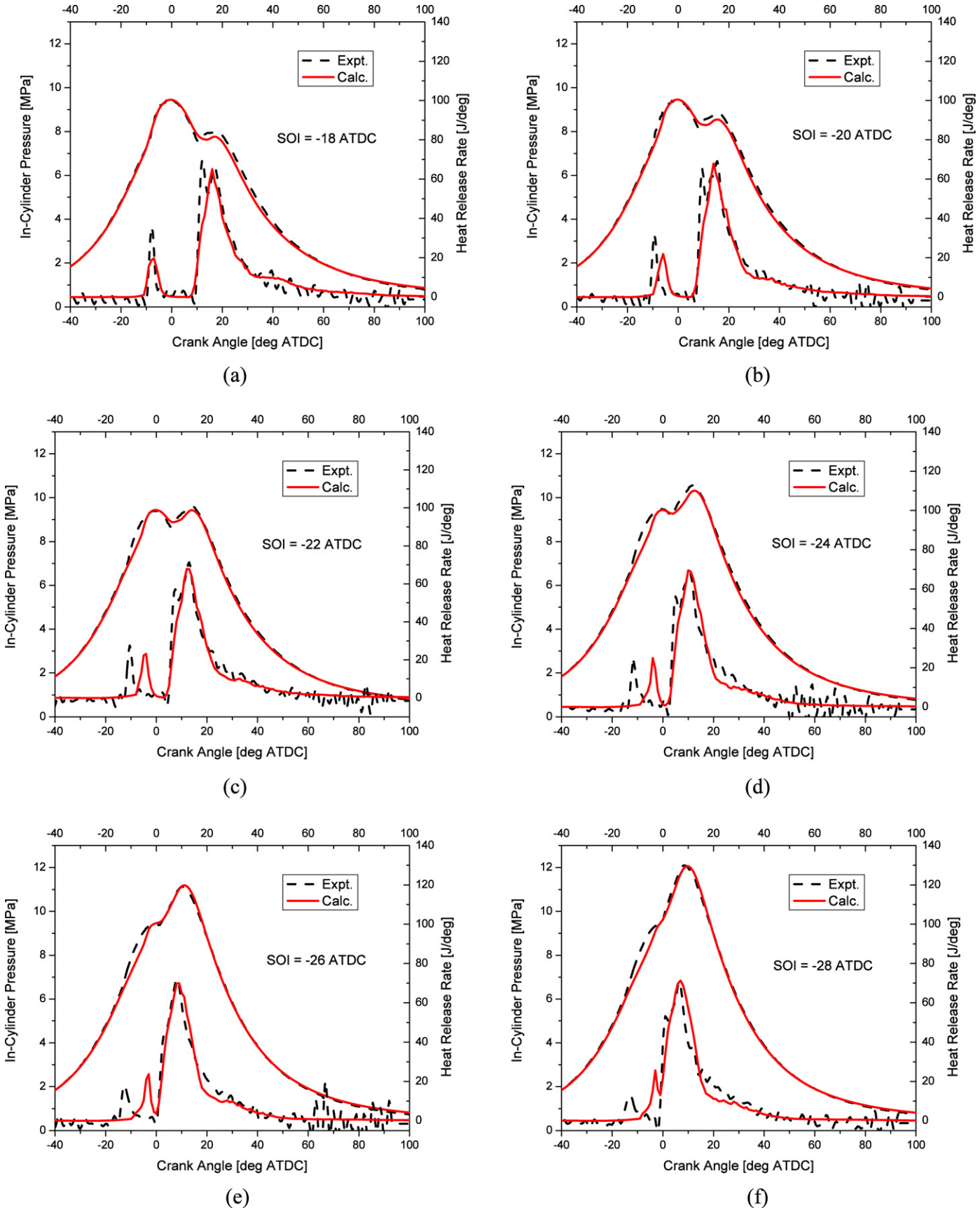

Fig. 7. Comparison of predicted and measured in-cylinder pressures and heat release rates for six cases of light-duty diesel engine: (a) SOI = −18; (b) SOI = −20; (c) SOI = −22; (d) SOI = −24; (e) SOI = −26; (f) SOI = −28 °CA ATDC.

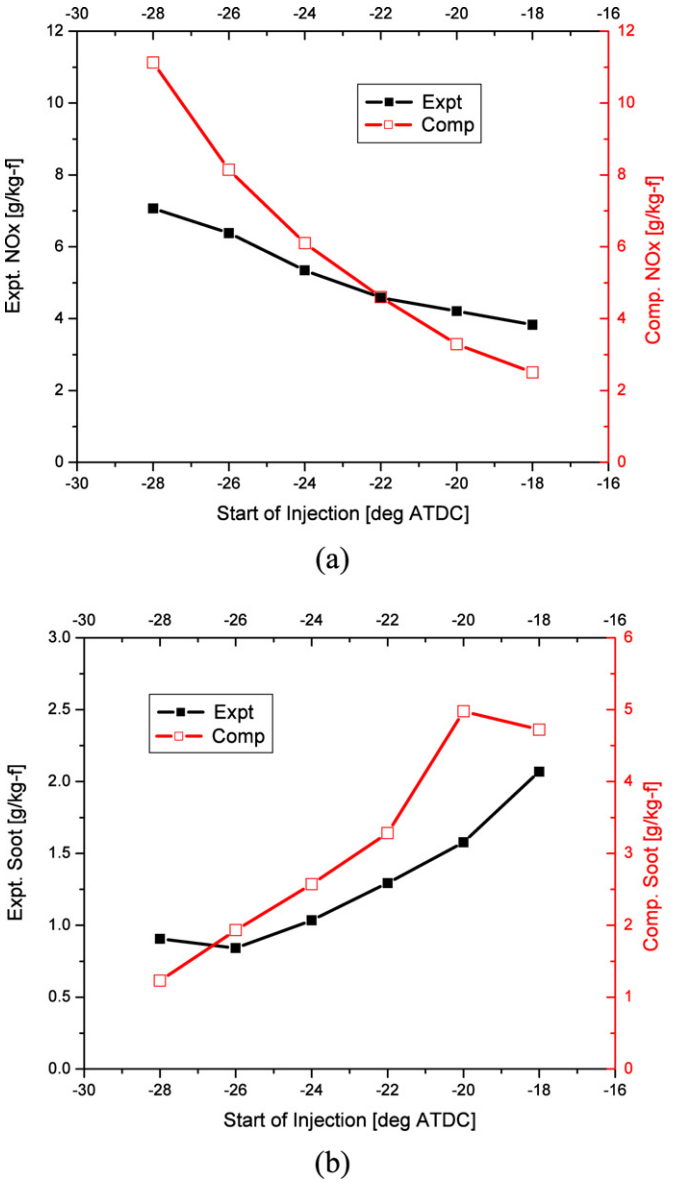

Fig. 8. Comparison of predicted engine-out and measured emissions for light-duty diesel engine: (a) NOx and (b) soot.

amples. The mass of soot particles is one of the quantities the nine-step soot model can predict. Some other important quantities, such as particle number, particle size, and intermediate species (acetylene and soot precursor), can be predicted by the nine-step model as well, which are discussed below.

6.1. Peak soot yield

As it has been shown in Fig. 3(b), the current nine-step soot model predicts higher peak soot yields, which are about 100 times higher than the engine-out soot. The prediction characterizes a distinct difference between the nine-step model and the two-step model. The previous study [17] demonstrated that the latter was only able to predict a lower peak soot yield—about 10 times higher than the engine-out soot. This observation is not unique to the benchmark engine case, but applicable to many other engines as well. Compared to the estimation made using a piecewise analysis on the heavy-duty diesel engine of same class [34], the nine-step model appears to be more consistent and realistic. Moreover, in terms of the response to the EGR effect, Fig. 3(b) suggests that the results are better predicted using the current nine-step model.

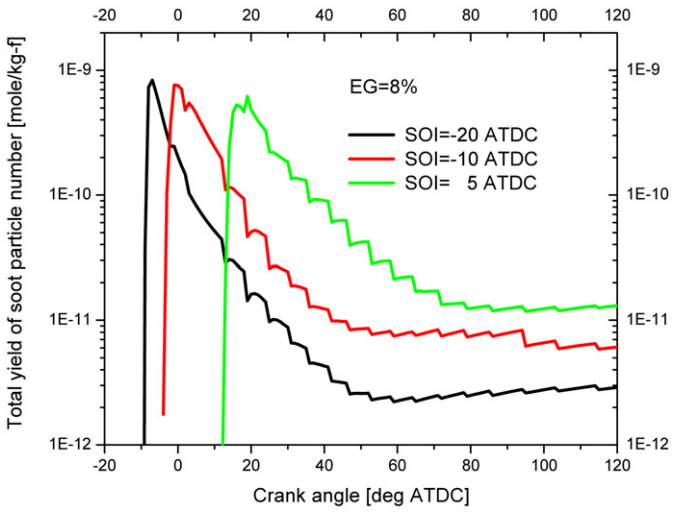

Fig. 9. Total yields of soot particle number predicted for three cases of Caterpillar heavy-duty diesel engine: SOI = −20, −10, and 5 °CA ATDC and EGR = 8%.

6.2. Soot particle number

It has been mentioned in the introduction section that to be able to predict soot particle number is another important feature of the nine-step phenomenological soot model. Although still unregulated, the particle number will soon be listed as the new target by the forthcoming regulation. As new diesel engines equipped with advanced technologies or combustion modes emit much less tailpipe PM emissions, the mass of PM emissions will eventually become a quantity difficult to be measured using the existing mass-based measuring techniques. Nonetheless, the particle number can be still a measurable quantity.

As an example, the predicted results of the Caterpillar heavy-duty diesel engine are selected for illustration. The total soot particle number yields, for three cases with different SOI timings (−20, −10, and 5 °CA ATDC) and EGR = 8% (see Table 3), are plotted in Fig. 9. Each of these three curves varies in a trend similar to that of the total soot mass (Fig. 3(b)). It increases rapidly at first due to high particle inception rates and, after its peak, reduces to a low level due to competition between particle formation (inception and growth) and particle destruction (coagulation and oxidation).

Particle inception is seen to be active for the whole engine process after the start of ignition. This observation is applicable not only to the early soot formation process but also to the late process during the expansion stroke. As shown in Fig. 9, the total number of soot particles continues to increase beyond 60 °CA ATDC, for example, for the case of SOI = −20 °CA ATDC.

The ratio between the peak and the engine-out of total soot particle number varies between 10 and 100. Although the SOI timings are different, the peaks of all three cases reach nearly the same level of magnitude. For the case of SOI = −20 °CA ATDC, the engine-out soot particle number is the lowest, whereas the highest for the case of SOI =5 °CA ATDC. For the former case, the ratio between the peak and the engine-out of soot particle number is about 100, whereas for the later only about 10. The predictions can be easily understood by combining the analysis of both Figs. 9 and 2. As shown in Fig. 2, advancing SOI enhances combustion intensity, leading to higher in-cylinder temperature that is beneficiary to soot oxidation, whereas retarding SOI results in relatively lower combustion intensity and soot oxidation rate, thus allowing more soot particles to survive in the late expansion stroke.

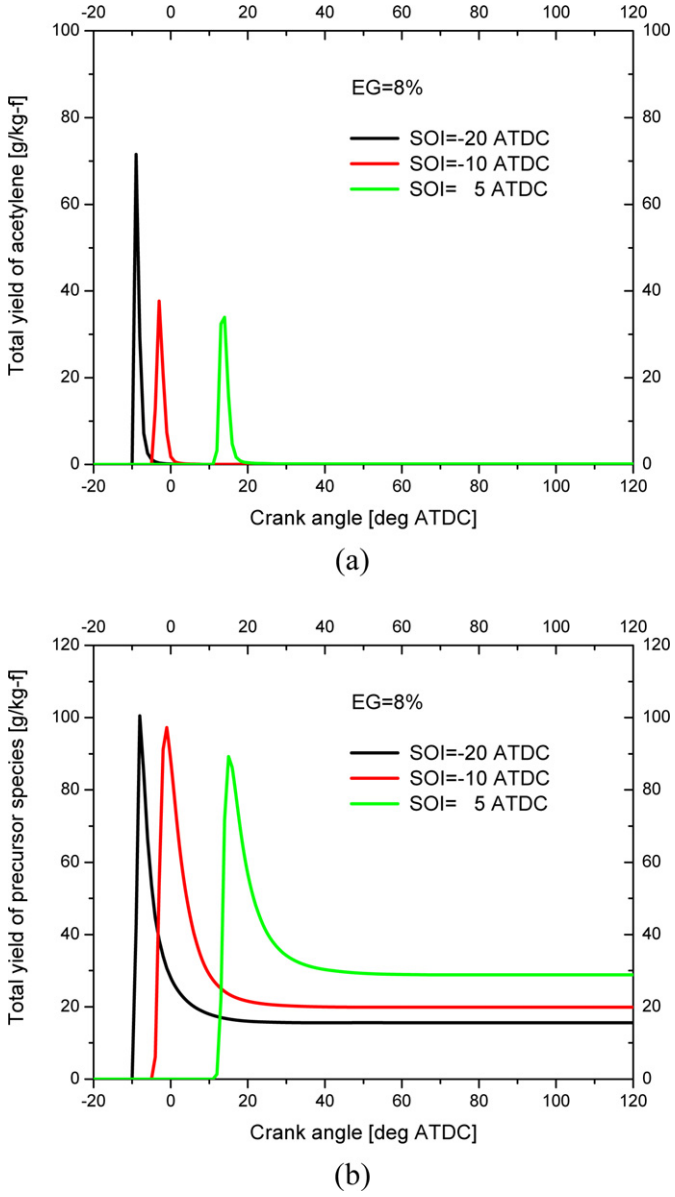

Fig. 10. Total yields of (a) acetylene and (b) soot precursor species predicted for three cases of Caterpillar heavy-duty diesel engine: SOI = −20, −10, and 5 °CA ATDC and EGR = 8%.

The observations discussed here are interesting but, nevertheless, further validations of the model in terms of soot particle number are still needed. At present, measuring the number and size of PMs emitted from diesel engines is still a challenging task. However, validations against the recently updated database measured in diesel-like facilities (e.g., [35–37]) can be set as an immediate step of future study.

6.3. Acetylene and soot precursor species

Acetylene and soot precursor are two intermediate species controlling the soot formation process. Meanwhile, they can be treated as unburnt hydrocarbons (UHCs), or as SOCs if needed.

For the same three cases as in Fig. 9, the predicted total yields of acetylene and soot precursor species are illustrated in Fig. 10. The figure suggests that the soot formation process spans merely a short period, during which the soot inception (particle number buildup) and the soot surface growth (particle mass buildup) are involved. This period corresponds to the first period around the

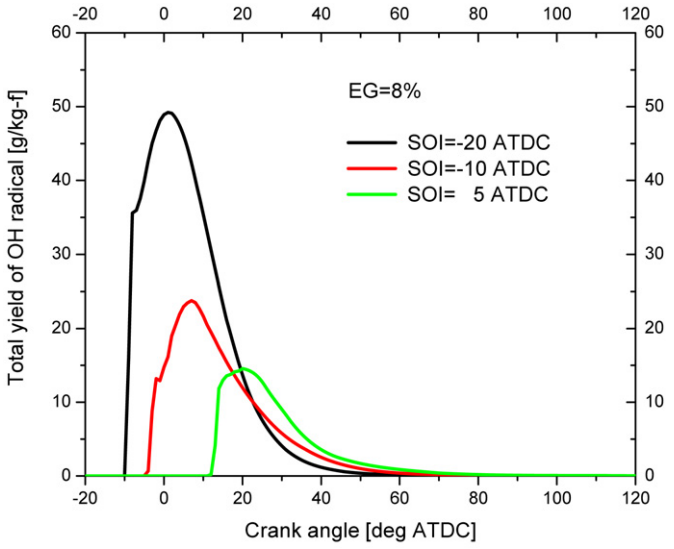

Fig. 11. Total yields of OH radical predicted for three cases of Caterpillar heavy-duty diesel engine: SOI = −20, −10, and 5 °CA ATDC and EGR = 8%.

peaks of the total soot mass yield (see, Fig. 3(b)) and of the total soot particle number yield (see, Fig. 9).

While acetylene survives only for a short period, the soot precursor tends to survive longer until to EVO. The predicted engine-out soot precursors with respect to SOI demonstrate the same trend as the soot mass (see Fig. 5). This result suggests that, if a relation describing the condensation of SOCs on the surfaces of soot particles could be established, the discrepancies observed for the engine-out soot mass might be easily corrected.

6.4. OH radical

As demonstrated in previous publication for the benchmark engine case [18], the OH radical distribution has been seen critical for controlling the soot particle distribution in a mixing-controlled diesel flame, particularly along the burning flame surfaces.

Here, Fig. 11 is an example used to illustrate the transient variation of total OH yields for the same three cases as in Figs. 9 and 10. The total OH yields are shown to vary largely for each of these cases, but comparison seems to indicate that the oxidation process does not affect much the inception of soot particles that controls the soot particle number (see Fig. 9). After the peak is reached, soot oxidation gains strength and dominates the soot formation and oxidation processes, which reduces the soot particle number down to lower levels.

Variation in OH yield indicates that soot oxidation is a controlling factor affecting the decays of total yields of both soot mass and particle number. The engine-out soot particle number is the lowest for the case of SOI = −20 °CA ATDC, but the highest for the case of SOI = 5 °CA ATDC. Nevertheless, the former corresponds to the highest OH production whereas the latter the lowest. The trend of engine-out soot mass agrees to the predictions of OH radical formed in the engines.

7. Conclusions

A nine-step phenomenological diesel soot model is described in this paper. The model, suitable to be coupled with the “Shell” ignition model and the characteristic time combustion (CTC) model, has been implemented into the ERC KIVA-3V code for predicting soot emissions in diesel engines. It can predict not only soot mass but also soot particle number. Validations have been conducted over a wide range of engine operating conditions, and two engines

(a heavy-duty diesel engine and a light-duty diesel engine) are selected as representative examples in the paper.

1. All the simulations were conducted using the same nine-step soot model without modification of rate constants. The performance of the model is assessed through comparison between the predictions and the measured mass-based soot emissions data. All the trends of the predicted engine-out soot are in agreement with measurements.
2. For low EGR cases, the soot model can lead to nearly accurate prediction. However, for high EGR cases, the simulations tend to under-predict the soot mass and a correction factor in a range of 2–3 is needed. The calibration of the model can be made by adjusting the model constants or by implementing a SOC condensation model.
3. The model has been used in previous publications [17,18] to investigate the soot distribution structure in a conventional, mixing-controlled flame. The prediction shows that the flame features a non-premixed, lifted flame, with a soot structure in agreement with Dec's conceptual model [33]. The prediction indicates that the nine-step model is fundamentally consistent with the physics and chemistry of soot formation and oxidation processes in diesel engines.
4. The nine-step phenomenological soot model predicts a higher peak soot yield, which is an order of magnitude higher than that by the two-step Hiroyasu's soot model.
5. The current and previous studies suggest that the model can be applied for diesel combustion analysis. It is computationally efficient, suitable to be integrated with genetic algorithms for engine system optimization.

Acknowledgements

The work was performed at the Engine Research Center, University of Wisconsin–Madison, being financially supported by Caterpillar, Inc. and the Ford Research Center in Aachen, Germany (FFA). The authors are grateful to Dr. Song-Charng Kong for help with the experimental data.

References

[1] H. Hiroyasu, T. Kadota, M. Arai, Development and use of a spray combustion modeling to predict diesel engine efficiency and pollutant emissions (Part I: Combustion modeling), Bulletin of the JSME 26 (1983) 569–575.
[2] J. Nagle, R.F. Strickland-Constable, Oxidation of carbon between 1000–2000 °C, Proc. 5th Carbon Conference 1 (1962) 154–164.
[3] M. Patterson, S.-C. Kong, G. Hampson, R.D. Reitz, Modeling the effects of fuel injection characteristics on diesel engine soot and NOx emissions, SAE Paper 940523, 1994.
[4] M. Kim, M.P. Liechty, R.D. Reitz, Application of micro-genetic algorithms for the optimization of injection strategies in a heavy-duty diesel engine, SAE Paper 2005-01-0219, 2005.
[5] A. Munnannur, S.-C. Kong, R.D. Reitz, Performance optimization of diesel engines with variable intake valve timing via genetic algorithms, SAE Paper 2005-01-0374, 2005.
[6] Y. Liu, A. Ali, R.D. Reitz, Simulation of effects of valve pockets and internal residual gas distribution on HSDI diesel combustion and emissions, SAE Paper 2004-01-0105, 2004.
[7] F. Tao, S. Srinivas, R.D. Reitz, D.E. Foster, Current status of soot modeling applied to diesel combustion simulations, in: Proceedings of COMODIA 2004, Yokohama, August 2–5, 2004.
[8] F. Tao, S. Srinivas, R.D. Reitz, D.E. Foster, Comparison of three soot models applied to multi-dimensional diesel combustion simulations, JSME International Journal, Series B 48 (2005) 71–678.
[9] J. Boulanger, F. Liu, W.S. Neill, G.J. Smallwood, An improved soot formation model for 3D diesel engine simulations, Journal of Engineering for Gas Turbines and Power 129 (2007) 877–884.
[10] A. Fusco, A.L. Knox-Kelecy, D.E. Foster, Application of a phenomenological soot model to diesel engine combustion, Proceedings of COMODIA 94 (1994) 571–576.
[11] A. Kazakov, D.E. Foster, Modeling of soot formation during DI diesel combustion using a multi-step phenomenological model, SAE Paper 982463, 1998.
[12] F. Tao, Y. Liu, B.H. RempelEwert, D.E. Foster, R.D. Reitz, D. Choi, P.C. Miles, Modeling the effects of EGR and injection pressure on soot formation in a high-speed direct-injection (HSDI) diesel engine using a multi-step phenomenological soot model, SAE Paper 2005-01-0121, 2005.
[13] K. Akihama, Y. Takatori, K. Inagaki, S. Sasaki, A.M. Dean, Mechanism of the smokeless rich diesel combustion by reducing temperature, SAE Paper 2001-01-0655, 2001.
[14] Y. Liu, F. Tao, D.E. Foster, R.D. Reitz, Application of a multiple-step phenomenological soot model to HSDI diesel multiple injection modeling, SAE Paper 2005-01-0924, 2005.
[15] A.A. Amsden, KIVA-3: A block-structured KIVA program for engines with vertical or canted valves, Report LA-13313-MS, Los Alamos National Laboratory, 1997.
[16] S.-C. Kong, Z. Han, R.D. Reitz, The development and application of a diesel ignition and combustion model for multi-dimensional engine simulation, SAE Paper 950278, 1995.
[17] F. Tao, D.E. Foster, R.D. Reitz, Soot structure in a conventional non-premixed diesel flame, SAE Paper 2006-01-0196, 2006.
[18] F. Tao, D.E. Foster, R.D. Reitz, Characterization of soot particle distribution in conventional, non-premixed DI diesel flame using a multi-step phenomenological soot model, Proceedings of Combustion Institute 31 (2007) 2991–2998.
[19] F. Tao, V.I. Golovitchev, J. Chomiak, A phenomenological model for the prediction of soot formation in diesel spray combustion, Combustion and Flame 136 (2004) 270–282.
[20] K.M. Leung, R.P. Lindstedt, W.P. Jones, A simplified reaction mechanism of soot formation in non-premixed flames, Combustion and Flame 87 (1991) 289–305.
[21] K.G. Neoh, J.B. Howard, A.F. Sarofim, Effect of oxidation on the physical structure of soot, in: 20th Symposium (International) on Combustion, The Combustion Institute, Pittsburgh, PA, 1974, pp. 951–957.
[22] Z. Han, R.D. Reitz, Turbulence modeling of internal combustion engines using RNG k–ε models, Combustion Science and Technology 106 (1995) 267–295.
[23] R.D. Reitz, R. Diwakar, Structure of high-pressure fuel sprays, SAE Paper 870598, 1987.
[24] R.D. Reitz, Modeling atomization processes in high-pressure vaporization sprays, Atomization and Spray Technology 3 (1987) 309–337.
[25] A.B. Liu, R.D. Reitz, Mechanism of air-assisted liquid atomization, Atomization and Sprays 3 (1993) 55–75.
[26] M.A. Patterson, Modeling the effects of fuel injection characteristics on diesel combustion and emissions, PhD Thesis, University of Wisconsin–Madison, 1997.
[27] Z. Han, R.D. Reitz, A temperature wall function formulation for variable-density turbulent flows with application to engine convective heat transfer modeling, International Journal of Heat and Mass Transfer 40 (1997) 613–625.
[28] Y.H. Zhu, R.D. Reitz, A 1-D gas dynamics code for subsonic and supersonic flows applied to predict EGR levels in a heavy-duty diesel engine, International Journal of Vehicle Design 22 (1999) 227–252.
[29] A.E. Klingbeil, Particulate and NOx reduction in a heavy-duty diesel engine using high levels of exhaust gas recirculation and very early or very late start of injection, MS Thesis, University of Wisconsin–Madison, 2002.
[30] N. Peters, J. Weber, The effects of spray formation and evaporation on mixing, auto-ignition and combustion in diesel engines, in: THIESEL 2006 Conference on Thermo- and Fluid Dynamic Processes in Diesel Engines, Valencia, Spain, September 12–15, 2006.
[31] T. Lee, R.D. Reitz, Response surface method optimization of a HSDI diesel engine equipped with a common rail injection system, Paper No. 2001-ICE-401, ICE, vol. 37-1, 2001 Fall Technical Conference, ASME, 2001.
[32] R.J. Donahue, Detailed in-cylinder engine data and evaluation of the potential for combustion control via manipulation of fuel and combustion chamber gas composition, PhD dissertation, University of Wisconsin–Madison, 1999.
[33] J.E. Dec, A conceptual model of DI diesel combustion based on laser-sheet imaging, SAE Paper 970873, 1997.
[34] P.F. Flynn, R.P. Durrett, G.L. Hunter, A.O. zur Loye, O.C. Akinyemi, J.E. Dec, C.K. Westbrook, Diesel combustion: An integrated view combining laser diagnostics, chemical kinetics, and empirical validation, SAE Paper 1999-01-0509, 1999.
[35] Engine Combustion Network, Sandia National Laboratories, http://public.ca.sandia.gov/ecn/, 2007.
[36] C.A. Idicheria, L.M. Pickett, Soot formation in diesel combustion under high-EGR conditions, SAE Paper 2005-01-3834, 2005.
[37] R.J. Crookes, G. Sivalingam, M.A.A. Nazha, H. Rajakaruna, Prediction and measurement of soot particulate formation in a confined diesel fuel spray-flame at 2.1 MPa, International Journal of Thermal Sciences 42 (2003) 639–646.